Flow strength of highly hydrated Mg- and Na-sulfate hydrate salts, pure and in mixtures with water ice, with application to Europa

William B. Durham,[1] Laura A. Stern,[2] Tomoaki Kubo,[1,3] and Stephen H. Kirby[2]

Received 27 April 2005; revised 13 July 2005; accepted 16 August 2005; published 21 December 2005.

[1] We selected two Europan-ice-shell candidate highly hydrated sulfate salts for a laboratory survey of ductile flow properties: $MgSO_4 \cdot 7H_2O$ (epsomite) and $Na_2SO_4 \cdot 10H_2O$ (mirabilite), called MS7 and NS10, respectively. Polycrystalline samples in pure form and in mixtures with water ice I were tested using our cryogenic high-pressure creep apparatus at temperatures $232 \leq T \leq 294$ K, confining pressures $P = 50$ and 100 MPa, and strain rates $4 \times 10^{-8} \leq \dot{\varepsilon} \leq 7 \times 10^{-5}$ s^{-1}. Grain size of NS10 samples was >100 μm. The flow strength σ of pure MS7 was over 100 times that of polycrystalline ice I at comparable conditions; that of pure NS10 over 20 times that of ice. In terms of the creep law $\dot{\varepsilon} = A\sigma^n e^{-Q/RT}$, where R is the gas constant, we determine parameter values of $A = 10^{12.1}$ MPa^{-n}s^{-1}, $n = 5.4$, and $Q = 128$ kJ/mol for pure NS10. Composites of ice I and NS10 of volume fraction ϕ_{NS10} have flow strength $\sigma_c = [\phi_{NS10}\sigma_{NS10}^J + (1 - \phi_{NS10})\sigma_{iceI}^J]^{1/J}$ where $J \approx -0.5$, making the effect on the flow of ice with low volume fractions of NS10 much like that of virtually undeformable hard rock inclusions. Being much stronger and denser than ice, massive sulfate inclusions in the warmer, ductile layer of the Europan ice shell are less likely to be entrained in convective ice flow and more likely to be drawn to the base of the ice shell by gravitational forces and eventually expelled. With only smaller, dispersed sulfate inclusions, at probable sulfate $\phi < 0.2$, the shell may be treated rheologically as pure, polycrystalline ice, with boundary conditions perhaps influenced by the high density and low thermal conductivity of the hydrated salts.

Citation: Durham, W. B., L. A. Stern, T. Kubo, and S. H. Kirby (2005), Flow strength of highly hydrated Mg- and Na-sulfate hydrate salts, pure and in mixtures with water ice, with application to Europa, *J. Geophys. Res.*, *110*, E12010, doi:10.1029/2005JE002475.

1. Introduction

[2] Highly hydrated sulfurous compounds spatter the surface of Europa. Near-infrared mapping of the Europan surface by the Galileo spacecraft showed that reddish disrupted terrains and linea (such as double ridges) have distorted water absorption bands suggestive of highly hydrated materials with very little free water present. *McCord et al.* [1998, 1999, 2002] attributed the spectra to hydrated magnesium sulfates or sodium carbonates on the basis of cosmochemistry and known IR absorption spectra. Sulfuric acid hydrate has also been implicated for Europa on the basis of both theory and spectroscopic observation [*Carlson et al.*, 2002, 1999; *Dalton et al.*, 2003; *McCord et al.*, 1998, 2002]. The presence of hydrated sulfate salts on and within icy moons had already been predicted by *Kargel* [1991] from the composition of carbonaceous chondrites. A thin and easily penetrated ice shell overlying a liquid ocean had been predicted since the earliest models of Europa [*Consolmagno and Lewis*, 1976]. Evidence of conducting oceans from Galileo magnetometer measurements [*Kivelson et al.*, 2000] has thus made the argument for the occurrence of hydrated sulfurous compounds on the surface of Europa very robust.

[3] Current models of the Europan crust [e.g., *Kargel et al.*, 2000; *Spaun and Head*, 2001] vary significantly in detail but generally agree on (1) an icy surface that has been resurfaced by salt-rich material in regions where crustal disruption or cracking are implied (roughly 50% of the surface); (2) an icy shell that may or may not have entrained heterogeneous zones or layers of denser (than ice) hydrated salts; and (3) a liquid ocean below the ice shell that is slightly to highly electrically conductive. Any remaining sulfurous compounds derived from the chondrites may also end up as a sub-ocean evaporite layer.

[4] The composition of a briny crust of Europa postulated by *Kargel* [1991] and discussed by *Hogenboom et al.* [1995] and *Kargel* [1998a, 1998b] is based on a model in which sulfates are leached out [*Fanale et al.*, 2001] of the carbonaceous chondritic material from which Europa presumably was accreted. *McKinnon and Zolensky* [2003] argue on the basis of more recent meteoritic analysis that sulfides rather than sulfates comprise the primitive chon-

[1]Lawrence Livermore National Laboratory, University of California, Livermore, California, USA.
[2]U.S. Geological Survey, Menlo Park, California, USA.
[3]Now at Department of Earth and Planetary Sciences, Faculty of Sciences, Kyushu University, Fukuoka, Japan.

0148-0227/05/2005JE002475$09.00

drites, and that the sulfates on Europa derived from hydrothermal alteration of these sulfides in Europa's primordial ocean. Since the sulfides are generally less water soluble than the sulfates, the end result is a much less salty ocean and ice shell. The evolution of Europa's icy component subsequent to accretion depends on the mechanical and thermal energy inputs and exchanges, differences in the physical properties of the brines and crystalline phases (such as density and rheology), and the physical chemistry and dynamics of this briny system. *Kargel* [1998a, 1998b] argues that fractional crystallization of these dense hydrates and their melts may also tend to enrich in briny hydrates the deeper part of Europa's ice layer. The processes that bring the brines to the surface, such as explosive volcanism, upward filling of opening-mode fractures and ice diapirism, may also tend to mix hydrates and ice.

[5] The question we investigate here is how the presence of hydrated sulfate salts might affect the ice rheology (read viscosity) in the Europan ice shell, and by extension, how other planetary structures may be affected where salts are present. If Europa's outer crust is indeed a shell of ice overlying a liquid ocean, then the thickness of the shell and type of geologic structures at the surface will depend on the rheology of the shell material [*McKinnon*, 1999; *Ojakangas and Stevenson*, 1989; *Pappalardo et al.*, 1998; *Ruiz and Tejero*, 2003; *Spaun and Head*, 2001]. The presence of the liquid ocean means that the temperatures at both the surface and base of the shell will be fixed, at roughly 100 K [e.g., *McKinnon*, 1999] and the melting point of the shell material, respectively, and therefore that the thickness of the ice shell will be determined by the shell's thermal [*Prieto-Ballesteros and Kargel*, 2005] and rheological properties. A rheologically soft shell favors convective cooling and thus low overall thermal gradients and a thicker shell, but at the same time is effective at generating heat by tidal dissipation [*Ojakangas and Stevenson*, 1989]. By contrast, a rheologically hard shell, a so-called conductive lid, might support higher temperature gradients and therefore be thin, but if it deforms only elastically under tidal stresses, it will not be heated by tidal flexing.

[6] With a surface temperature near 100 K, the near-surface portion of the Europan ice shell is essentially undeformable [e.g., *Durham and Stern*, 2001] on the 10^7- to 10^9-year age scale of the surface [*Pappalardo et al.*, 1999]. The shell is thus likely to be rheologically layered, with a conductive lid overlying a convective lower layer. On the basis of the weakest credible ice rheology, that of grain-size-sensitive creep [*Goldsby and Kohlstedt*, 2001] at a grain size of about 1 mm, convection could be maintained in the lower part of a shell as thin as 10–30 km [*McKinnon*, 1999; *Pappalardo et al.*, 1998]. It has also been suggested that diapiric upwelling can penetrate the conductive lid, and explain the round, dome-like or disrupted surface features known as lenticulae [*Carr et al.*, 1998; *Pappalardo et al.*, 1999, 1998; *Ruiz and Tejero*, 2003; *Sotin et al.*, 2002; *Spaun and Head*, 2001]. The linea, including fracture-like cycloidal features, which on the basis of geographical relationships to sulfates [*McCord et al.*, 1998, 1999, 2002] also represent shell penetrations and a brittle lid, are consistent with tidal forces in an ice shell [*Greeley et al.*, 1998; *Greenberg et al.*, 2002]. How these "fractures" penetrate a ductile ice layer is unclear.

2. Choice of Sample Material and Sample Preparation

[7] *Kargel* [1991] predicted that the dominant sulfate on Europa should be $MgSO_4 \cdot 12H_2O$ and $Na_2SO_4 \cdot 10H_2O$ (mirabilite), which we designate here MS12 and NS10, respectively, on the basis of chondritic compositions as discussed above and on sulfate-water phase diagrams. *McCord et al.* [1998, 1999, 2002] identified spectral similarities in the Europan near-infrared to those of combinations of MS6 (hexahydrate), MS7 (epsomite), NS10, $Na_2Mg(SO_4)_2 \cdot 10H_2O$ (bloedite), and $Na_2CO_3 \cdot 10H_2O$ (natron). *Dalton et al.* [2005a, 2005b] carried out the most thorough lab study to date of hydrate spectra, including that of the problematic MS12 (see below). They concluded, as did McCord and coworkers, that the Europan spectra represented a complex mix of hydrated salts, but saw better approximations to Europan spectra with increasing hydration numbers, with the spectra of MS12 being the most "Europa-like."

[8] Sample complexity bedevils laboratory deformation experiments, whose purposes are best served by relevant, simple (e.g., monomineralic) materials. We fell short of this ideal in the case of MS12, whose synthesis in the lab turned out not to be straightforward. The binary system $MgSO_4$–H_2O has been carefully studied at elevated pressure by *Hogenboom et al.* [1995]. On the water-rich side it exhibits a shallow ice-hydrate eutectic and various hydrates form from magnesium sulfate-rich liquids over different temperature intervals (Figure 1). MS12 and ice I are the stable crystalline phases at and below the eutectic point to pressures of 200 MPa. At higher pressures, the denser ice polymorphs are in equilibrium with MS12. At 100 MPa, corresponding to a depth of about 100 km on Europa, the eutectic melting temperature is depressed by about 12 K from its room-pressure value.

[9] Efforts to synthesize MS12 by cooling the stoichiometrically correct quantities of MS7 + H_2O did not meet with immediate success because of the metastability of MS7. Rather than react to form MS12, the mixture of MS7 and liquid solution tends to bypass the peritectic reaction at 275 K, and instead additional MS7 is formed and the composition of the liquid follows the metastable extension of the liquidus. At the metastable MS7-H_2O eutectic point at ~268 K, the reaction L → ice + MS7 occurs (Figure 1). J. Kargel (personal communication, 2001) suggested temperature cycling between 268 K and 275 K to encourage the growth of MS12 crystals, a technique subsequently demonstrated by *Dalton et al.* [2005b]. In the interests of expeditious execution of a survey of hydrated sulfates, we therefore chose to use readily available reagent grade MS7 and the somewhat more hydrated NS10 (mirabilite, reagent grade), and mixtures of the latter with laboratory-grown, pure water ice I.

3. Methods

[10] We measure the ductile flow strength of low melting temperature planetary materials using a gas deformation

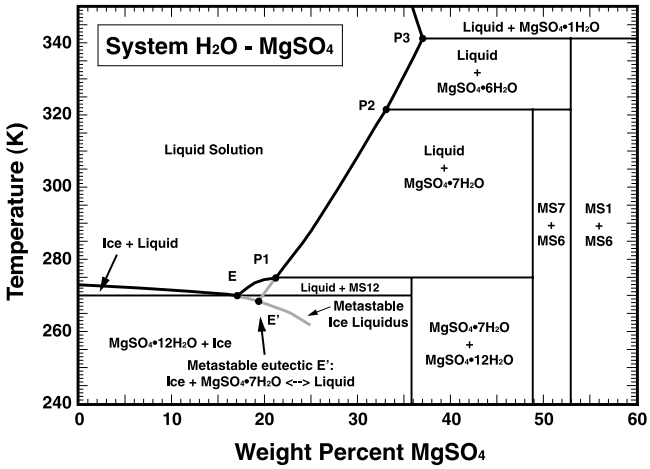

Figure 1. A 1-atm phase diagram for the H_2O-rich side of the H_2O-$MgSO_4$ system. Points P1–P3 are peritectics, and E and E' are eutectics. From *Hogenboom et al.* [1995]. See color version of this figure in the HTML.

apparatus immersed in a cryostat. Sample and pressure vessel have cylindrical symmetry. Gas pressure simulates geologic overburden P to provide a confinement that suppresses brittle fracture. The sample itself is encapsulated in a soft metal (indium) jacket to exclude the gas pressure medium from the sample, allowing the gas to effectively confine the sample. An axial piston sliding through dynamic seals at a displacement rate $\dot{u}$ provides the compressional end load that shortens the sample plastically. The force of the piston on the end of the sample is measured by an internal load cell (Figure 2), and the advancement of the piston is measured by external displacement transducers on the moving piston. More details are given by *Heard et al.* [1990].

[11] Generally, the deformation that results in such circumstances is nearly uniform, i.e., a pore-free sample that begins as a cylinder finishes as a shorter cylinder with the same volume (Figure 2 shows a sample after deformation). We refer to the amount of deformation as strain or shortening ε, which we give the engineering definition of change in length divided by starting length. We seek to define the rheology, or constitutive flow law, of the solid by measuring the relationship between the variables differential stress σ, which is the applied end load divided by sample cross-sectional area, and strain rate $\dot{\varepsilon} = \dot{u}/L$, where L is the current length of the sample, at conditions of fixed pressure P and temperature T. The canonical form of the relationship describing steady state creep is

$$\dot{\varepsilon} = A\sigma^n e^{-\left(E^* + PV^*\right)/RT}, \qquad (1)$$

where R is the gas constant and A, n, E^*, and V^* are material- and deformation mechanism-specific flow parameters, called the preexponential constant, the stress exponent, the activation energy, and the activation volume, respectively. Where the quantity PV^* changes little (as happens here, see below), we can simplify the activation energy to $Q = E^* + PV^*$.

[12] We tested pure, granulated, reagent grade MS7 and NS10 as well as mixtures of NS10 and H_2O ice I. We handled the pure salts in a humid glove box at room temperature, disaggregating clumps of granules by hand with mortar and pestle, spooning the loose granules into indium "cans," tamping lightly, then sealing the cans. The

Figure 2. Sample assembly after deformation, inverted for photographic purposes. The length of the entire assembly is about 225 mm. The 56-mm-long sample, a 60:40 NS10:H_2O mixture by volume, is contained in the slightly irregular portion of the cylindrical indium encapsulation at the top. Although the sample has been shortened by 16% (Table 1), its diameter is smaller than that of the rest of the column because of the effect of hydrostatic compaction on the initially porous mixture. The fact that the form of the sample is only slightly irregular is testimony that the strain has been nearly uniform. The narrow column of steel below the sample is the internal force gage, whose elastic change in length gives a direct measure of the force on the sample. The wide portion at the base is the high-pressure plug. See color version of this figure in the HTML.

indium jacket can be seen in Figure 2. Grain sizes were not measured or carefully controlled. We estimate that the bulk of the starting material was of grain diameter 0.1–0.5 mm.

[13] Mixed NS10 + H_2O samples were prepared in a similar manner, but in a freezer at T ~ 240 K. Appropriate amounts of granulated NS10 and H_2O were weighed and then ground and mixed together using mortar and pestle. Grinding was more aggressive than for the pure material, proceeding for several minutes and interspersed with frequent stirring, folding, and scraping of the material to achieve a uniform mix. Final consistency of the material was nearly flour-like, suggesting grain sizes of the order of a few tens of micrometers, thus considerably finer than that of the pure material. As discussed below, we attempted imaging of these materials by scanning electron microscopy to determine grain size and degree of phase mixing, but met with only limited success. Indium cans were filled and sealed as above.

[14] To create the pore-free compacts needed for creep testing, we preceded deformation with a warm, hydrostatic press of the samples at 100 MPa, at room temperature in the case of the pure materials, and at 250 K for the ice mixtures (warmer temperatures allow the possibility of significant grain growth (S. M. McDaniel et al., Grain growth in polycrystalline fine-grained laboratory ice Ih, manuscript in preparation 2005). Porosity was determined from measurements of starting mass and current volume. Volume was measured immediately after the pre-deformation compaction step for the one MS7 sample and first NS10 sample by removing the assembly from the vessel, and at the completion of deformation for all samples, with results given below. The predominant source of uncertainty was the caliper measurement of diameter at various locations on the slightly rumpled jacket (e.g., Figure 2), leading to an uncertainty in volume of roughly 0.5 cm^3 of a total volume of 20–25 cm^3.

[15] The usual experimental approach to solving equation (1) is to treat one or the other of σ and $\dot{\varepsilon}$ as the dependent variable, holding the other independent variables constant. Thus with T and P fixed, one sets a constant $\dot{\varepsilon}$ and measures the σ response (called a constant strain rate test), or sets constant σ and measures $\dot{\varepsilon}$ (called a creep test). In the presumption of steady state, the observed relationship between $\dot{\varepsilon}$ and σ should be the same in either mode. We used both modes in these experiments, although never changed modes in a given experiment. Our creep tests were strictly constant σ, with actual load corrected steadily upwards during deformation to compensate for cross-sectional area broadening. Our constant strain rate tests were in fact constant $\dot{u}$, meaning that $\dot{\varepsilon}$ increased slightly (since L decreased slightly) during the tests.

[16] All runs involved stepping. Once the relationship between $\dot{\varepsilon}$ and σ gave good indication that it was no longer evolving with strain, i.e., that "apparent" steady state had been reached, we often changed one of the independent variables in order to glean more than one measurement from a given sample. Establishing true steady state is a major undertaking, and must include detailed microstructural studies as well as deformation tests to very high strain. For the present purpose of surveying unknown rheologies, the current methodology is probably satisfactory.

[17] Microscopic examination of deformed samples of pure NS10 and NS10 + ice mixtures was carried out by cryogenic scanning electron microscopy (SEM) using a Gatan Alto 2100 cryo-preparation and coating station attached to the sample chamber of a LEO 982 field emission SEM. Specimens in the instrument were held under vacuum at $T < 100$ K at all times during preparation, transfer, and examination to preserve volatile materials and prevent contamination by condensed water from the atmosphere. The surfaces we imaged in this study were fresh fracture surfaces created by cleaving within the cryo-station.

4. Measurements and Observations

[18] We tested seven samples. One was pure MS7, three were pure NS10, and three were mixtures of ice plus NS10. Conditions, testing mode (creep or constant $\dot{u}$), and results are listed in Table 1. The MS7 sample, which we tested first, exhibited such extraordinarily high strength compared with that of ice I that it would appear essentially undeformable in any mixture with an appreciable amount of ice. Since we have already surveyed the rheology of ice I plus undeformable inclusions [*Durham et al.*, 1992], we dedicated the balance of this experimental work to the somewhat softer NS10 and its mixtures with ice.

4.1. Pure MS7

[19] MS7, Run 466 in Table 1, tested in constant displacement rate mode, showed very high strength (Figure 3a), requiring deforming forces almost beyond the capability of an instrument designed primarily for deforming planetary ices. The porosity measurements suggest that most of the shortening reflected in Figure 3a was related to porosity reduction rather than ductile flow. We calculated the relative change in porosity (which is somewhat more precise than the absolute measurement) from the end of deformation step 2 to the end of step 6 to be 0.035 ± 0.01, and the absolute porosity at the conclusion of the run (after step 6) to be 0 ± 0.025. The diameter of the sample expanded very slightly during steps 3–6, so to accommodate the porosity collapse, the length shortening must have been slightly greater than 0.035 ± 0.01. The measured shortening strain from steps 3–6 was 0.031, leading to the conclusion that much, if not all, the shortening resulted from porosity collapse. Thus we plot the "flow" of MS7 in the manner of other materials here, with the caveat that the true flow strength of MS7 is probably higher than represented in Figure 3a. On the log $\dot{\varepsilon}$ versus log σ plot of Figure 3a, the true strength of MS7 at a given T and $\dot{\varepsilon}$ should thus plot to the right of the values shown.

4.2. Pure NS10

[20] The porosity of the first pure NS10 sample following hydrostatic compaction was zero within 2–3% uncertainty, so by extension we assume that porosity at the start of deformation was zero for all NS10 and mixed NS10 + ice samples. Three samples of pure NS10 were tested at temperatures from 232 K to room temperature in both creep and constant displacement rate mode. Results are listed in Table 1 and plotted in Figure 3b. Of the 16 deformation steps listed in Table 1, three were not plotted because stress and/or strain rate continued to evolve significantly with strain, or because the magnitude of strain in the step was very small.

Table 1. Run Data[a]

Run	Sample	Mode	*P*, MPa	*T*, K	ε	$\dot{\varepsilon}$, s^{-1}	σ, MPa
466(1)	MS7	const $\dot{u}$	50	294.0	0.030	3.55×10^{-6}	52.0 ± 8.0
466(2)	MS7	const $\dot{u}$	50	294.0	0.058	3.66×10^{-7}	29.0 ± 3.0
466(3)	MS7	const $\dot{u}$	50	293.5	0.064	VNP	VNP
466(4)	MS7	const $\dot{u}$	50	293.0	0.077	7.00×10^{-8}	23.0 ± 2.0
466(5)	MS7	const $\dot{u}$	100	293.5	0.082	3.75×10^{-7}	46.0 ± 5.0
466(6)	MS7	const $\dot{u}$	100	284.5	0.089	3.78×10^{-7}	93.0 ± 5.0
467(1)	NS10	const $\dot{u}$	50	293.0	0.035	3.60×10^{-4}	VNP
467(2)	NS10	const $\dot{u}$	50	293.0	0.066	3.73×10^{-5}	14.0 ± 1.0
467(3)	NS10	const $\dot{u}$	50	275.0	0.100	3.87×10^{-6}	20.5 ± 1.0
467(4)	NS10	const $\dot{u}$	50	275.0	0.141	4.05×10^{-6}	26.0 ± 1.0
467(5)	NS10	const $\dot{u}$	50	239.5	0.148	4.09×10^{-7}	52.0 ± 2.0
467(6)	NS10	const $\dot{u}$	50	259.5	0.157	4.13×10^{-7}	26.0 ± 2.0
467(7)	NS10	const $\dot{u}$	50	259.5	0.194	4.32×10^{-6}	36.0 ± 2.0
472(1)	NS10	creep	100	249.5	0.022	VNP	VNP
472(2)	NS10	creep	100	249.5	0.091	2.58×10^{-6}	45.6 ± 0.5
472(3)	NS10	creep	50	250.0	0.121	2.06×10^{-6}	46.3 ± 0.7
472(4)	NS10	creep	100	232.5	0.128	3.73×10^{-8}	53.0 ± 1.0
472(5)	NS10	creep	100	232.5	0.158	2.07×10^{-6}	77.0 ± 0.5
472(6)	NS10	creep	100	250.0	0.192	2.47×10^{-6}	46.8 ± 0.5
473(1)	60:40 NS10:H_2O	creep	100	232.5	0.061	3.26×10^{-6}	15.9 ± 0.6
473(2)	60:40	creep	100	232.5	0.106	2.26×10^{-6}	14.0 ± 1.0
473(3)	60:40	creep	100	232.5	0.197	3.82×10^{-5}	23.1 ± 0.4
473(4)	60:40	creep	100	232.5	0.230	6.39×10^{-6}	15.7 ± 1.0
474(1a)	80:20	creep	100	232.0	0.020	5.67×10^{-7}	30.7 ± 0.8
474(1b)	80:20	creep	100	233.0	0.049	1.01×10^{-6}	31.5 ± 0.8
474(2)	80:20	creep	100	232.5	0.120	2.13×10^{-5}	46.8 ± 0.5
474(3)	80:20	creep	100	232.5	0.138	5.90×10^{-7}	29.5 ± 0.6
474(4)	80:20	creep	100	232.0	0.168	2.90×10^{-6}	37.5 ± 0.4
475(1)	40:60	creep	100	232.5	0.053	7.17×10^{-7}	6.1 ± 0.5
475(2)	40:60	creep	100	232.5	0.126	1.13×10^{-5}	11.6 ± 0.2
475(3)	40:60	creep	100	232.5	0.156	1.10×10^{-6}	5.8 ± 0.1
508(1)	NS10	const $\dot{u}$	50	293.0	0.057	7.51×10^{-6}	8.9 ± 0.3
508(2)	NS10	const $\dot{u}$	50	293.0	0.063[b]	3.67×10^{-6}	8.3 ± 0.5
508(3)	NS10	const $\dot{u}$	50	293.0	0.260	7.21×10^{-5}	14.5 ± 0.5

[a]VNP denotes values changing significantly with time; not plotted.
[b]Strain interval $\Delta\varepsilon = 0.006$ too short; not plotted.

[21] We looked for gross effects of confining pressure *P* (indicating a large value for *V** in equation (1)) in these hydrated sulfate salts and found none. The final two steps of MS7 sample 466 were conducted at 100 MPa, versus 50 MPa for the others, and showed no significant effects (e.g., compare 466(1) and 466(5) in Table 1). Four of the NS10 steps were run at a confinement of 100 MPa; nine were at 50 MPa. In the only direct comparison on the same sample, back-to-back steps 472(2) and 472(3) at 100 and 50 MPa, respectively, showed slight strengthening accompanying the pressure decrease. Otherwise, no significant trend with pressure is obvious. For curve-fitting purposes, therefore, we combined the activation enthalpy $E^* + PV^*$ in equation (1) to a single activation energy *Q* appropriate for all pressures. Multivariate fit results for both MS7 and NS10 to this revised form of equation (1) are given in Table 2. The fits plot as the straight lines in Figure 3. Even at the deepest part of a 100-km-thick Europan crust *P* is roughly 100 MPa, so *P* probably need not be included explicitly in models of ductile flow of the sulfates in the ice shell or in a putative layer at the base of the ocean.

[22] The planetary implications become clearer when the strength of MS7 and NS10 are compared with that of water ice (Figure 4), where the enormous viscosity contrast between ice and the hydrated sulfates is evident. Figure 4 is an Arrhenius plot, which samples a different two-dimensional slice of three-variable space than does Figure 3. In this view, higher flow strength plots higher on the vertical axis. Recall that the MS7 points are probably lower bounds for its strength. The contrast in apparent viscosity, i.e., the ratio of strain rates at a given differential stress and temperature, between NS10 and ice is over 5 orders of magnitude, and between MS7 and NS10 is an additional few orders of magnitude.

4.3. Ice + NS10 Mixtures

[23] The survey of the rheology of mixtures of ice and NS10 was done with mixtures of three compositions, vol%NS10:vol%ice I = 40:60, 60:40, and 80:20. The deformation mode was creep and all tests were conducted at $T = 233$ K and $P = 100$ MPa. Results are plotted in Figure 5. The trend from pure NS10 through the several mixtures blends smoothly into the strength of pure polycrystalline ice I deforming by dislocation creep [*Durham and Stern*, 2001]. It can be seen in Figure 5 that the value of the stress exponent *n* in equation (1), which on a logarithmic scale is inversely proportional to the distance between lines of constant $\dot{\varepsilon}$, decreases monotonically from the value for pure NS10 ($n = 5.4$) to that for ice ($n = 4$).

4.4. SEM Observations

[24] We looked at fracture sections from samples 472, 474, 475, and 508, the first and last being pure NS10 and

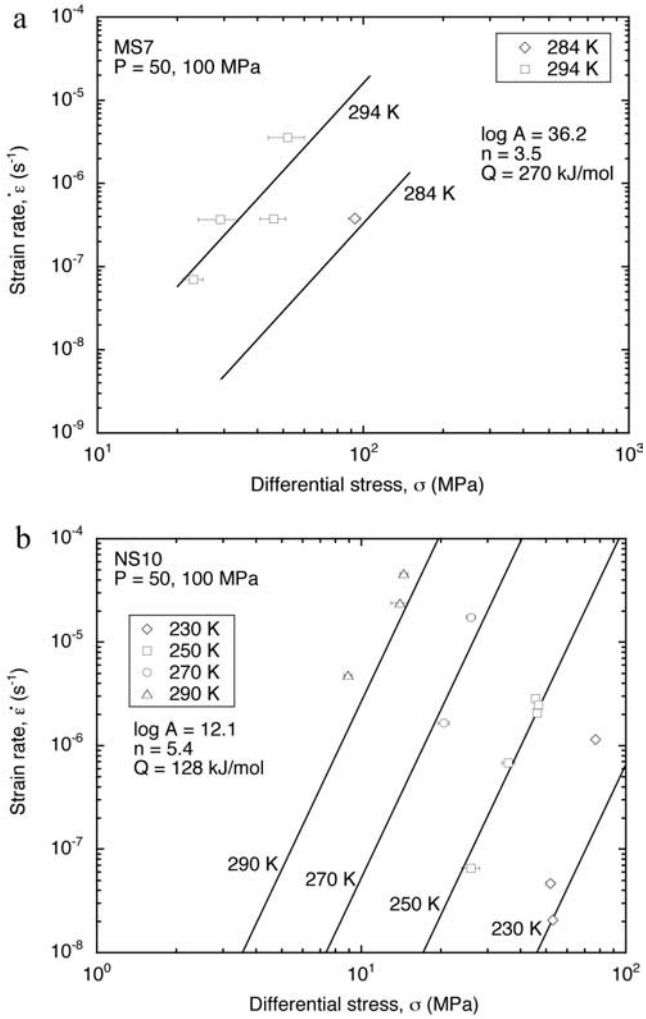

Figure 3. Strength data for (a) MS7 and (b) NS10 plotted as log $\dot{\varepsilon}$ versus log σ. The individual points are measured values (from Table 1), and the straight lines are the best fits given in Table 2. For plotting purposes, the positions of the points have been shifted very slightly (using the parameters in Table 2) to account for the $\leq$1 K shift between labeled T on the plot and actual T (Table 1). Much of the strain in the MS7 samples (Figure 3a) can be accounted for by porosity collapse, so the values here are lower bounds for strength (see text for details). See color version of this figure in the HTML.

the middle two mixtures of ice + NS10. Our success in the SEM was limited. First, we found that the surface appearance of NS10 changes rapidly under vacuum despite SEM chamber temperatures < 100 K (Figure 6). Regularly spaced pores and crack-like voids cover surfaces within a few tens of minutes of operation. Their regular spacing and crystallographically controlled morphologies suggest shrinkage and thus a dewatering reaction. The reaction occurs everywhere, not just in regions examined, so the cause is apparently not beam damage. Second, fracture surfaces formed for examination are more disrupted and littered with debris than with other icy materials we have examined. We were unable to do satisfactory imaging of mixtures of ice + NS10 (Figure 7). The techniques for good imaging of highly hydrated sulfates in SEM are non trivial, and are currently undergoing development in our laboratory. Recently, *McCarthy et al.* [2003, 2004] have had good success imaging eutectic structures in sulfate-water systems using cryo-SEM, revealing complex intergrowths of phases in patterns quite unlike the physical mixtures we created for this study (Figure 7).

[25] The crystallographic control of desiccation pattern has the benefit of allowing us to distinguish grains. On the basis of images such as Figure 6b we conclude that grain diameters of the pure NS10 samples are on the order of a few 100 μm, which is consistent with the starting size of the loose granules that make up the pure NS10 samples. Grain size of the ice + NS10 samples is likely to be smaller because of the more aggressive grinding during preparation, but we have not found a means for distinguishing phase or grain size from images such as Figure 7.

5. Discussion

5.1. Deformation Mechanisms

[26] The large grain sizes of the pure NS10 samples and the high value of stress exponent n for that material (Table 1) indicate that the dominant mechanism of deformation of the pure NS10 here is dislocation creep, a mechanism that is grain-size-insensitive (GSI). Water ice and a number of silicate materials have demonstrated that, under conditions of very small grain size (usually <10 μm) and low stress, a regime of grain-size-sensitive (GSS) creep with n values closer to 2 can produce measurable strain at laboratory timescales [see, e.g., *Rutter and Brodie*, 2004] and references therein for further reading on GSS creep in geological materials). Identification of mechanism is relevant because at the low stresses typical of geological and planetary settings, GSS creep mechanisms potentially dominate deformation. The reason for this is clear from equation (1): Given two mechanisms for generating $\dot{\varepsilon}$, both operating simultaneously but one more stress-sensitive (i.e., of higher n) than the other, the proportion contributed by the lower-n mechanism will increase as σ decreases.

[27] Direct measurement of grain size for the mixed ice + NS10 samples is elusive, but Figure 5 suggests strongly that GSS creep was not important in these tests, since high n values are maintained for all mixtures. Anecdotally, creating test samples of sufficiently small grain size to activate significant GSS creep usually takes extraordinary means.

Table 2. Multivariate Fit Parameters to $\dot{\varepsilon} = A\sigma^n e^{-Q/RT}$

Material	Number of Points	Log A, MPa^{-n}s^{-1}	n	Q, J/mol	Multicorrelation Coefficient (R)
MS7	5	36.2	3.5	270000	0.89
NS10	13	12.1	5.4	128000	0.94

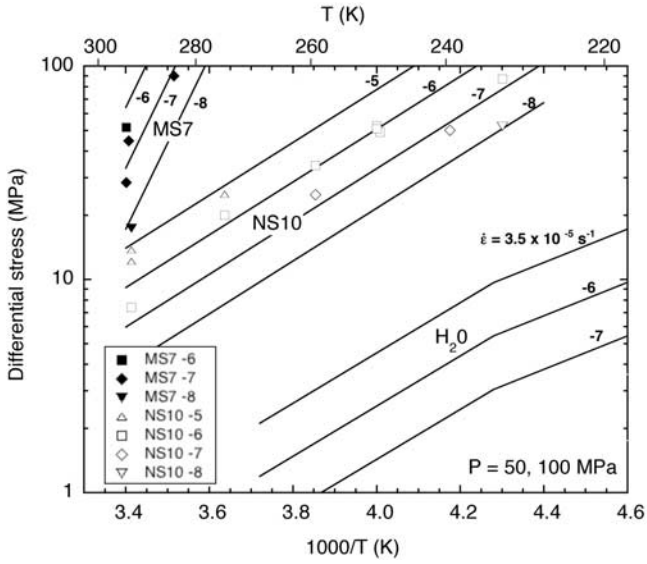

Figure 4. Comparison of strengths of pure MS7, NS10, and H_2O ice I plotted on an Arrhenius diagram of log σ versus inverse *T*. Measurement data from Table 1 plotted here are the same plotted in Figure 3. Flow laws in this projection are drawn as lines of constant $\dot{\varepsilon}$ at the values labeled, with the lines for each material separated by 1 order of magnitude in $\dot{\varepsilon}$. Parameters for MS7 and NS10 are the best fits in Table 2. Parameters for ice are taken from *Durham and Stern* [2001]. The differential stress required to deform NS10 at a given $\dot{\varepsilon}$ and *T*, i.e., its strength, is a factor of 20 or more higher than that for ice at comparable conditions. The viscosity contrast, i.e., the increase in $\dot{\varepsilon}$ at a given σ and *T*, is over 5 orders of magnitude. MS7 in turn is far stronger than even the NS10. Given that the MS7 flow law is probably a lower bound on strength, the contrast is likely to be even greater than that represented here. Compared with ice, MS7 can be considered essentially undeformable. See color version of this figure in the HTML.

In particular, simple mechanical grinding is rarely sufficient and is demonstrably insufficient for ice [*Goldsby and Kohlstedt*, 2001; *Rutter and Brodie*, 2004].

5.2. Rheology of Mixtures

[28] The data of Figure 5 for one strain rate are compared with simple models for rheology of two-phase mixtures in Figure 8. It can be shown [*Tullis et al.*, 1991] that the strength of a mixture must be bounded by two cases: isostrain rate (i.e., both phases experience the same strain rate), wherein strength is a maximum bound; and isostress (both phases experience the same stress), wherein strength is a minimum bound.

[29] The rheology of polyphase mixtures is difficult to model in a general way owing to the number of parameters that must be known. In addition to volume fractions and flow laws for end-member phases, grain shapes, geometrical arrangements, and lattice preferred orientation can influence the strength of the aggregate. Special phase-to-phase interactions such as dispersion hardening [*Arzt et al.*, 2001], grain boundary pinning [*Baker and Gerberich*, 1979; *Hooke et al.*, 1972], and enhanced grain boundary diffusion rates [*Bruhn et al.*, 1999] affect the strength of the aggregate in ways that the end-member flow laws cannot predict. Empirical models therefore outnumber theoretical [*Jordan*, 1987; *Takeda*, 1998; *Treagus*, 2002; *Tullis et al.*, 1991]. Best model behavior and understanding of refinements (such as effects of grain shapes and orientation) appear when the two phases have nearly similar rheologies. As rheological contrast increases, models generally tend toward either singularities or, as noted by *Tullis et al.* [1991], the isostress bound.

[30] At a viscosity contrast between NS10 and ice of $\sim 10^5$, low volume fractions of NS10 can be treated by the theory of dilute suspensions of rigid spheres [see, e.g., *Ji*, 2004], whose flow strength follows a law of the form

$$\sigma_{\text{ice I+NS10}} = \sigma_{\text{pure ice I}}(1-\phi)^{-2.5}, \tag{2}$$

where φ is the volume fraction of inclusions. Except at very low values of φ, say <0.2, Equation (2) does a poor job of matching the rheology of NS10 + ice (Figure 8). A better fit to the measurements is the empirical relationship found by *Durham et al.* [1992] for the flow of ice + hard sand particulates for sand fractions $0 \leq \phi \leq 0.56$,

$$\sigma_{\text{ice I+particulates}} = \sigma_{\text{pure ice I}}\, e^{b\phi}, \tag{3}$$

where *b* is a constant ≈ 2 (Figure 8). Above φ = 0.56, the sand forms a connected network, and strength rises rapidly.

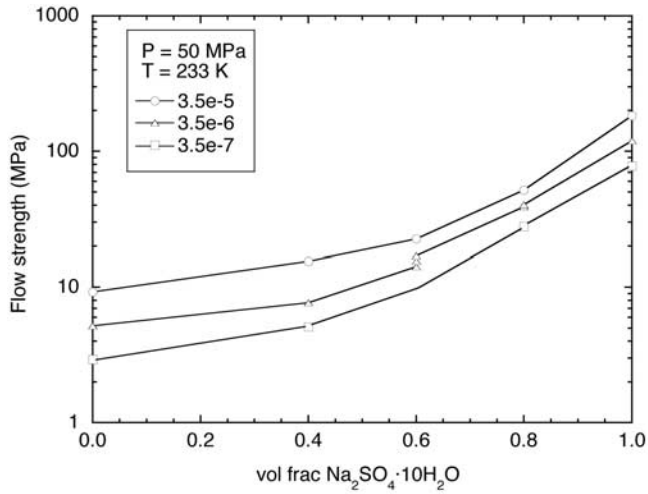

Figure 5. Flow strength of mixtures of NS10 + ice at fixed *T* = 233 K and three fixed values of $\dot{\varepsilon}$ separated by 1 order of magnitude. Data are from Table 1. Tabulated values of σ are adjusted slightly for plotting purposes to the nearest $\dot{\varepsilon}$ listed in the legend using equation (1) and an appropriate stress exponent *n*. For NS10 mixtures of volume fraction 0.8 and 1.0, where the flow of NS10 appears to dominate, we used *n* = 5 (near the 5.4 value in Table 2); for the other mixtures we used *n* = 4, the value for pure ice I [*Durham and Stern*, 2001]. The effect of using *n* = 4 versus *n* = 5 can be no worse than roughly 6%, which is approximately the size of the symbols. See color version of this figure in the HTML.

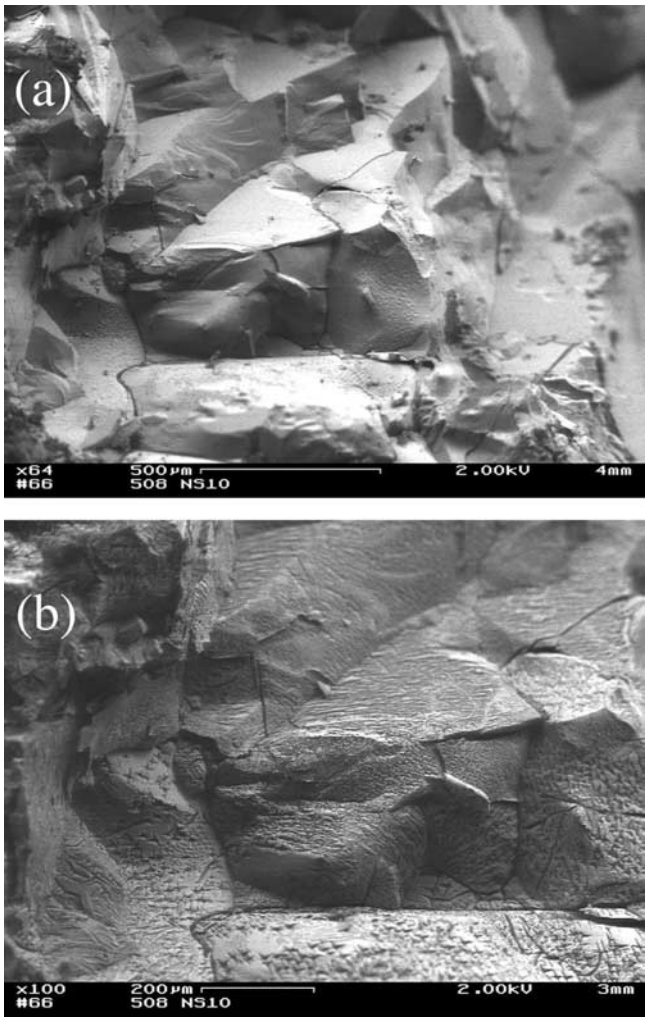

Figure 6. (a) Fracture section through pure NS10 sample 508 as imaged by cryo-SEM shortly after introduction into the SEM vacuum chamber, and (b) the same region at slightly higher magnification 30 min later. All surfaces are etched with pits and crack-like voids that are apparently crystallographically controlled. We suspect that a dewatering reaction is responsible for the etching. Individual grains are apparent from different etching patterns, and suggest that grains are at least as large as the large, blocky pieces that have loosened from one another. Grain diameters of a few hundred micrometers are thus indicated. Scale bar in Figure 6a is 500 μm, and in Figure 6b is 200 μm.

[31] Interestingly, a more satisfactory fit for all values of ϕ, which also takes into account the finite strength of the harder NS10, is the relationship

$$M_c(J) = \left[\sum_{i=1}^{N} \left(\phi_i M_i^J\right)\right]^{1/J}, \qquad (4)$$

asserted by *Ji* [2004] and *Ji et al.* [2004] to be a generalized mixture rule for any specific mechanical property M (such as flow strength). The subscript c refers to the composite property, and i refers to the ith phase. J is a scaling parameter that accounts for grain shapes and geometric

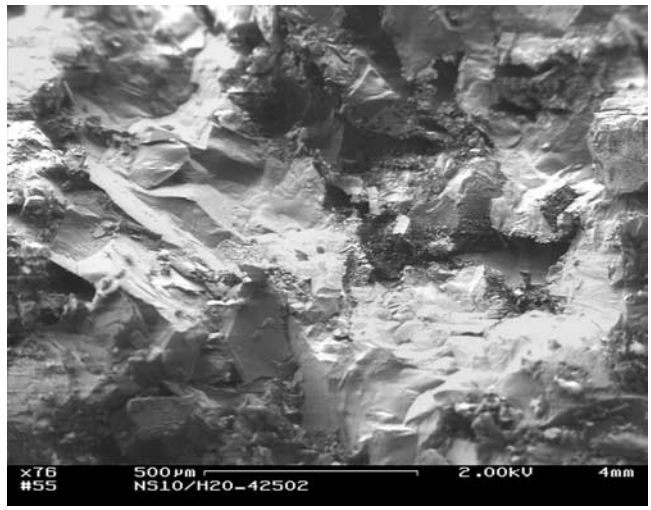

Figure 7. Fracture section through sample 474, a 80:20 mix by volume of NS10:ice I at low magnification. The irregular surface makes identification of grain sizes difficult. Illumination is by secondary electrons, and shadowing from the irregular surface also interferes with phase contrast information, so distinguishing ice grains from NS10 grains is also difficult. Work to improve imaging techniques with this material is ongoing. Scale bar is 500 μm.

arrangements. For spherical hard inclusions in a soft matrix $J = -0.5$ should give the best fit; likewise, for spherical soft inclusions in a hard matrix, $J = 0.5$ is best. *Ji et al.* [2004] find that, while not universal, the most typical behavior in two-phase rock mixtures is a gradation of J from -0.25 to $+0.25$ as the volume fraction ϕ_s of the hard phase increases from 0 to 1, with most of the change occurring in the range $0.5 < \phi_s < 0.7$. For our NS10 + ice I mixtures, a single value

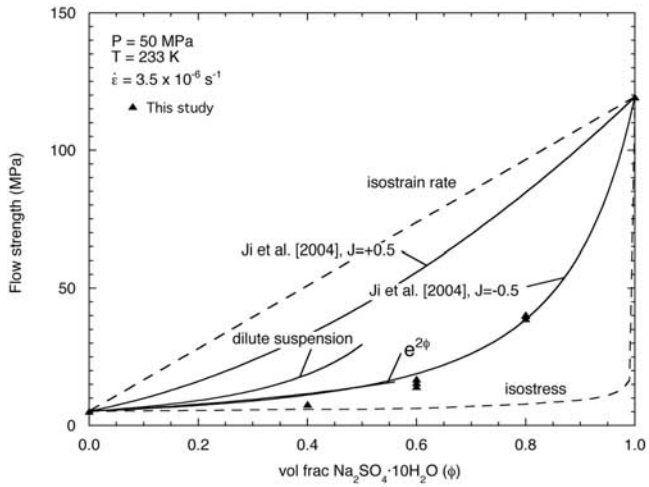

Figure 8. Flow at $\dot{\varepsilon} = 3.5 \times 10^{-6}$/s (triangles) compared with various models for rheology of mixtures discussed in text. Isostrain rate and isostress are theoretical bounds. The label $e^{2\phi}$ is the empirical dependence for ice + undeformable inclusions applicable to $0 \leq \phi \leq 0.56$ [*Durham et al.*, 1992]. See color version of this figure in the HTML.

of $J = -0.5$ gives good agreement with all observed values (Figure 8). A fixed value of J is not unprecedented. For example, the flow strength of mixtures of ice I + ammonia dihydrate $NH_3 \cdot 2H_2O$ [*Durham et al.*, 1993], wherein the ice I is the harder phase, follows equation (4) with a near single-valued $J = -0.6$.

[32] At this point, J is an empirical parameter. It embodies little deformation physics that would render the extrapolation of laboratory flow law to (much slower) planetary strain rates more robust. Hopefully this situation will improve as the systematics identified by J help us learn more about the flow of multiphase solids.

6. Planetary Implications: Europa

[33] The extension of these reconnaissance results to the planets is tenuous, given the breadth of the field and sparseness of data. Other species of hydrated compounds are probable on Europa besides those studied here [*Dalton et al.*, 2005b; *Kargel*, 1991; *McCord et al.*, 2002]. Also, we know little about the rheological effects of compositional and textural complexities brought about by ordinary geologic processes. However, the strength contrasts observed here may be so large as to override other complications. We may infer from our results that all highly hydrated Na- and Mg-sulfate salts are stronger than ice, since all are basically SO_4 tetrahedra, Na- or $Mg(H_2O)_6$ octahedra, and H_2O groups bonded by covalent sharing of polyhedral points and varying degrees of hydrogen bonding [*Hawthorne et al.*, 2000]. If this inference is correct, we may then surmise that the Europan ice shell is composed of an ice matrix with second-phase inclusions (i.e., the hydrated salts) that are much more dense (ρ = 1.46 Mg/m^3 for NS10, 1.51 for MS12, 1.68 for MS7 [e.g., *Kargel*, 1991]), much less thermally conductive [*Prieto-Ballesteros and Kargel*, 2005], and for the warm layer, far less deformable, than the matrix.

[34] It is difficult to perceive how such inclusions could persist as large, discrete volumes in the deformable layer. The inclusions are negatively buoyant in ice, so only the rapid convection of the ice layer would prevent salts already present from sinking to the bottom of the shell, and from there decoupling from the shell and falling to the base of the ocean. By Stokes flow [e.g., *Turcotte and Schubert*, 1982], only smaller inclusions will be entrained in such convective flow. The relevance to the current work is that because of their high strength, the inclusions are less likely to be deformed into higher aspect ratio shapes (at the extreme: from spheres to plates) that would be more prone to convective entrainment or more prone to being stretched and pulled to smaller sizes. Here we do not calculate the maximum inclusion size in the ductile layer of the shell, but suggest that it is probably smaller than the smallest geologic features we perceive on the surface. One is led to the conclusion that whatever the sulfate content of the Europan ice shell, it is present mostly as dispersed, small inclusions, or as eutectic structures such as imaged by *McCarthy et al.* [2003, 2004]. By the results for mixtures shown in Figure 5, and given that the buoyancy of the shell means that its total sulfate content cannot exceed roughly 0.2 by volume, the deformable layer of the shell must behave rheologically approximately like pure, polycrystalline ice.

[35] A corollary to this conclusion is that the only morphological expression at the surface of the solid sulfate in the interior will be related to the higher density and lower thermal conductivity of sulfate. Diapirism, for example, cited above as an emplacement mechanism for lenticulae on the Europan surface, can be calculated as the flow of an ice diapir through ice of different density. As another example, because of its lower thermal conductivity, a sulfate-rich region will have a different temperature gradient and therefore different viscosity than its lateral surroundings. Gradient, viscosity, and density all affect the Rayleigh number and likelihood of convective instability [e.g., *Turcotte and Schubert*, 1982]. Given that density and temperature will be related and that density has its own effect on convective instability, a modeling exercise may well show variations with monotonically changing sulfate content that become more and less stable with respect to surrounding ice-rich zones.

[36] Regarding the cryovolcanic hydrated sulfurous compounds associated with linea, lenticulae, and chaos terrains on the Europan surface, there is probably little relevance of ductile strength to local geology except perhaps when magmas are first emplaced and still warm, since even ice near at 100 K is cold and undeformable. If surface material is recycled on the 50 My timescale favored by *Pappalardo et al.* [1999], then massive salt deposits will eventually leave the shell as discussed above, or be dispersed in the icy convective layer.

7. Conclusions

[37] Our laboratory strength measurements show that epsomite (MS7) and mirabilite (NS10) are orders of magnitude more viscous than ice I at similar conditions (Figure 4), and that mixtures of NS10 + ice begin to show significant strengthening with respect to pure ice only when the NS10 content is well over 0.5 by volume (Figure 5). If other hydrated salts have similar properties, and if the considerable extrapolation in strain rate from lab to very slow planetary rates is valid, then, while massive hydrated salt formations will be rheologically distinct from ice, ice layers containing dispersed material will not be. Because of their high density and inability to deform in convective flows with ice, it seems unlikely that massive hydrated sulfate salts could remain in the Europan ice shell, but would rather have returned to the putative internal ocean or to the base of the crust below the ocean.

[38] **Acknowledgments.** We wish to thank Christine McCarthy for reading the manuscript and helping us better understand metastabilities in the system $MgSO_4$-H_2O. We also thank Michael Carr and two anonymous reviewers for their helpful comments and input. This work was supported by NASA under order W-19,868. T. K. acknowledges support of JSPS Postdoctoral Fellowships for Research Abroad (Japan). Work was performed under the auspices of the U.S. Department of Energy by the Lawrence Livermore National Laboratory under contract W-7405-ENG-48.

References

Arzt, E., G. Dehm, P. Gumbsch, O. Kraft, and D. Weiss (2001), Interface controlled plasticity in metals: Dispersion hardening and thin film deformation, *Prog. Mater. Sci.*, *46*(3–4), 283–307.

Baker, R. W., and W. W. Gerberich (1979), The effect of crystal size and dispersed-solid inclusions on the activation energy for creep of ice, *J. Glaciol.*, *24*, 179–194.

Bruhn, D. F., D. L. Olgaard, and L. N. Dell'Angelo (1999), Evidence for enhanced deformation in two-phase rocks: Experiments on the rheology of calcite-anhydrite aggregates, *J. Geophys. Res.*, *104*(B1), 707–724.

Carlson, R. W., R. E. Johnson, and M. S. Anderson (1999), Sulfuric acid on Europa and the radiolytic sulfur cycle, *Science*, *286*(5437), 97–99.

Carlson, R. W., M. S. Anderson, R. E. Johnson, M. B. Schulman, and A. H. Yavrouian (2002), Sulfuric acid production on Europa: The Radiolysis of sulfur in water ice, *Icarus*, *157*(2), 456–463.

Carr, M. H., et al. (1998), Evidence for a subsurface ocean on Europa, *Nature*, *391*(6665), 363–365.

Consolmagno, G. J., and J. S. Lewis (1976), Structural and thermal models of icy Galilean satellites, in *Jupiter*, edited by T. Gehrels, pp. 1035–1051, Univ. of Ariz. Press, Tucson.

Dalton, J. B., R. Mogul, H. K. Kagawa, S. L. Chan, and C. S. Jamieson (2003), Near-infrared detection of potential evidence for microscopic organisms on Europa, *Astrobiology*, *3*(3), 505–529.

Dalton, J. B., C. S. Jamieson, R. C. Quinn, O. Prieto-Ballesteros, and J. Kargel (2005a), Cryogenic reflectance spectroscopy of highly hydrated sulfur-bearing salts, paper presented at Lunar and Planetary Science Conference XXXVI, Lunar and Planet. Inst., Houston, Texas.

Dalton, J. B., O. Prieto-Ballesteros, J. Kargel, C. S. Jamieson, J. Joliviet, and R. Quinn (2005b), Spectral comparison of highly hydrated sulfate salts to disrupted terrains on Europa, *Icarus*, *177*(2), 472–490.

Durham, W. B., and L. A. Stern (2001), Rheological properties of water ice—Applications to satellites of the outer planets (review), *Annu. Rev. Earth Planet. Sci.*, *29*, 295–330.

Durham, W. B., S. H. Kirby, and L. A. Stern (1992), Effects of dispersed particulates on the rheology of water ice at planetary conditions, *J. Geophys. Res.*, *97*(E12), 20,833–20,897.

Durham, W. B., S. H. Kirby, and L. A. Stern (1993), Flow of ices in the ammonia-water system, *J. Geophys. Res.*, *98*(B10), 17,667–17,682.

Fanale, F. P., Y. H. Li, E. De Carlo, C. Farley, S. K. Sharma, K. Horton, and J. C. Granahan (2001), An experimental estimate of Europa's "ocean" composition independent of Galileo orbital remote sensing, *J. Geophys. Res.*, *106*(E7), 14,595–14,600.

Goldsby, D. L., and D. L. Kohlstedt (2001), Superplastic deformation of ice: Experimental observations, *J. Geophys. Res.*, *106*(B6), 11,017–11,030.

Greeley, R., et al. (1998), Europa: Initial Galileo geological observations, *Icarus*, *135*(1), 4–24.

Greenberg, R., P. Geissler, G. Hoppa, and B. R. Tufts (2002), Tidal-tectonic processes and their implications for the character of Europa's icy crust, *Rev. Geophys.*, *40*(2), 1004, doi:10.1029/2000RG000096.

Hawthorne, F. C., S. V. Krivovichev, and P. C. Burns (2000), The crystal chemistry of sulfate minerals, in *Sulfate Minerals: Crystallography, Geochemistry, and Environmental Significance*, edited by C. N. Alpers, J. L. Jambor, and D. K. Nordstrom, pp. 1–112, Mineral. Soc. of Am., Washington, D. C.

Heard, H. C., W. B. Durham, C. O. Boro, and S. H. Kirby (1990), A triaxial deformation apparatus for service at $77 \leq T \leq 273$ K, in *The Brittle-Ductile Transition in Rocks*, *Geophys. Monogr. Ser.*, vol. 56, edited by A. G. Duba et al., pp. 225–228, AGU, Washington D. C.

Hogenboom, D. L., J. S. Kargel, J. P. Ganasan, and L. Lee (1995), Magnesium sulfate-water to 400 MPa using a novel piezometer: Densities, phase equilibria, and planetological implications, *Icarus*, *115*, 258–277.

Hooke, R. L., B. B. Dahlin, and M. T. Kauper (1972), Creep of ice containing dispersed fine sand, *J. Glaciol.*, *11*, 327–336.

Ji, S. C. (2004), A generalized mixture rule for estimating the viscosity of solid-liquid suspensions and mechanical properties of polyphase rocks and composite materials, *J. Geophys. Res.*, *109*, B10207, doi:10.1029/2004JB003124.

Ji, S. C., Q. Wang, B. Xia, and D. Marcotte (2004), Mechanical properties of multiphase materials and rocks: A phenomenological approach using generalized means, *J. Struct. Geol.*, *26*(8), 1377–1390.

Jordan, P. G. (1987), The deformational behavior of bimineralic limestone halite aggregates, *Tectonophysics*, *135*(1–3), 185–197.

Kargel, J. (1998a), Physical chemistry of ices in the outer solar system, in *Solar System Ices*, edited by B. Schmitt, C. de Bergh, and M. Festou, pp. 3–32, Springer, New York.

Kargel, J. S. (1998b), The salt of Europa, *Science*, *280*, 1211–1212.

Kargel, J. S. (1991), Brine volcanism and the interior structures of asteroids and icy satellites, *Icarus*, *94*, 368–390.

Kargel, J. S., J. Z. Kaye, J. W. Head, G. M. Marion, R. Sassen, J. K. Crowley, O. P. Ballesteros, S. A. Grant, and D. L. Hogenboom (2000), Europa's crust and ocean: Origin, composition, and the prospects for life, *Icarus*, *148*, 226–265.

Kivelson, M. G., K. K. Khurana, C. T. Russell, M. Volwerk, R. J. Walker, and C. Zimmer (2000), Galileo magnetometer measurements: A stronger case for a subsurface ocean at Europa, *Science*, *289*, 1340–1343.

McCarthy, C. M., S. H. Kirby, W. B. Durham, and L. A. Stern (2003), Melt-grown grain textures of eutectic mixtures of water ice with magnesium- and sodium-sulfate hydrates and sulfuric-acid hydrate using cryogenic SEM (CSEM), *Eos Trans. AGU*, *84*(46), Fall Meet. Suppl., Abstract T42A-0275.

McCarthy, C. M., S. H. Kirby, W. B. Durham, and L. A. Stern (2004), Microstructure and physical properties of sulfate hydrate/ice eutectic aggregates in the binary system sodium-sulfate/water at planetary conditions, *Eos Trans. AGU*, *85*(47), Fall Meet. Suppl., Abstract P31A-0955.

McCord, T. B., et al. (1998), Salts an Europa's surface detected by Galileo's Near Infrared Mapping Spectrometer, *Science*, *280*, 1242–1245.

McCord, T. B., et al. (1999), Hydrated salt minerals on Europa's surface from the Galileo near-infrared mapping spectrometer (NIMS) investigation, *J. Geophys. Res.*, *104*(E5), 11,827–11,851.

McCord, T. B., G. Teeter, G. B. Hansen, M. T. Sieger, and T. M. Orlando (2002), Brines exposed to Europa surface conditions, *J. Geophys. Res.*, *107*(E1), 5004, doi:10.1029/2000JE001453.

McKinnon, W. B. (1999), Convective instability in Europa's floating ice shell, *Geophys. Res. Lett.*, *26*, 951–954.

McKinnon, W. B., and M. E. Zolensky (2003), Sulfate content of Europa's ocean and shell: Evolutionary considerations and some geological and astrobiological implications, *Astrobiology*, *3*(4), 879–897.

Ojakangas, G. W., and D. J. Stevenson (1989), Thermal state of an ice shell on Europa, *Icarus*, *81*, 220–241.

Pappalardo, R. T., et al. (1998), Geological evidence for solid-state convection in Europa's ice shell, *Nature*, *391*, 365–368.

Pappalardo, R. T., et al. (1999), Does Europa have a subsurface ocean? Evaluation of the geological evidence, *J. Geophys. Res.*, *104*(E10), 24,015–24,055.

Prieto-Ballesteros, O., and J. S. Kargel (2005), Thermal state and complex geology of a heterogeneous salty crust of Jupiter's satellite, Europa, *Icarus*, *173*, 212–221.

Ruiz, J., and R. Tejero (2003), Heat flow, lenticulae spacing, and possibility of convection in the ice shell of Europa, *Icarus*, *162*, 362–373.

Rutter, E. H., and K. H. Brodie (2004), Experimental grain size-sensitive flow of hot-pressed Brazilian quartz aggregates, *J. Struct. Geol.*, *26*(11), 2011–2023.

Sotin, C., J. W. Head, and G. Tobie (2002), Europa: Tidal heating of upwelling thermal plumes and the origin of lenticulae and chaos melting, *Geophys. Res. Lett.*, *29*(8), 1233, doi:10.1029/2001GL013844.

Spaun, N. A., and J. W. Head (2001), A model of Europa's crustal structure: Recent Galileo results and implications for an ocean, *J. Geophys. Res.*, *106*(E4), 7567–7575.

Takeda, Y. T. (1998), Flow in rocks modelled as multiphase continua: Application to polymineralic rocks, *J. Struct. Geol.*, *20*(11), 1569–1578.

Treagus, S. H. (2002), Modelling the bulk viscosity of two-phase mixtures in terms of clast shape, *J. Struct. Geol.*, *24*(1), 57–76.

Tullis, T. E., F. G. Horowitz, and J. Tullis (1991), Flow laws of polyphase aggregates from end-member flow laws, *J. Geophys. Res.*, *96*(B5), 8081–8096.

Turcotte, D. L., and G. Schubert (1982), *Geodynamics, Applications of Continuum Physics to Geological Problems*, 449 pp., John Wiley, Hoboken, N. J.

W. B. Durham, Lawrence Livermore National Laboratory, University of California, L-201, P. O. Box 808, Livermore, CA 94550, USA. (durham1@llnl.gov)

S. H. Kirby and L. A. Stern, U.S. Geological Survey, MS 977, 345 Middlefield Road, Menlo Park, CA 94025, USA.

T. Kubo, Department of Earth and Planetary Sciences, Faculty of Sciences, 33 Kyushu University, Fukuoka, 812-8581, Japan.